Boise State University

ScholarWorks

Materials Science and Engineering Faculty Publications and Presentations

Micron School for Materials Science and Engineering

10-2020

Impact of Arsenic Species on Self-Assembly of Triangular and Hexagonal Tensile-Strained GaAs(111)A Quantum Dots

Christopher F. Schuck
Boise State University

Kevin D. Vallejo
Boise State University

Trent Garrett
Boise State University

Qing Yuan
Hebei University

Ying Wang
Hebei University

See next page for additional authors

This is the Accepted Manuscript version of an article accepted for publication in *Semiconductor Science and Technology*. IOP Publishing Ltd is not responsible for any errors or omissions in this version of the manuscript or any version derived from it. The Version of Record is available online at https://doi.org/10.1088/1361-6641/aba6e0

Authors

Christopher F. Schuck, Kevin D. Vallejo, Trent Garrett, Qing Yuan, Ying Wang, Baolai Liang, and Paul J. Simmonds

This article is available at ScholarWorks: https://scholarworks.boisestate.edu/mse_facpubs/575

This is an author-produced, peer-reviewed version of this article. The final, definitive version of this document can be found online at *Semiconductor Science and Technology*, published by IOP Publishing. Copyright restrictions may apply. https://doi.org/10.1088/1361-6641/aba6e0.

IMPACT OF ARSENIC SPECIES ON SELF-ASSEMBLY OF TRIANGULAR AND HEXAGONAL TENSILE-STRAINED GaAs(111)A QUANTUM DOTS

Christopher F. Schuck,[1] Kevin D. Vallejo,[1] Trent Garrett,[2] Qing Yuan,[3] Ying Wang,[3] Baolai Liang,[3] and Paul J. Simmonds[1,2†]

[1] *Micron School of Materials Science & Engineering, Boise State University, Boise, Idaho 83725, USA*

[2] *Department of Physics, Boise State University, Boise, Idaho 83725, USA*

[3] *College of Physics Science & Technology, Hebei University, Baoding 071002, P.R. China*

† E-mail address: paulsimmonds@boisestate.edu

We use dimeric arsenic (As_2) or tetrameric arsenic (As_4) during molecular beam epitaxy to manipulate the structural and optical properties of GaAs(111)A tensile-strained quantum dots (TSQDs). Choice of arsenic species affects nucleation and growth behavior during TSQD self-assembly. Previously, epitaxial GaAs(111)A TSQDs have been grown with As_4, producing TSQDs with a triangular base, and "A-step" edges perpendicular to the three $\langle\bar{1}\bar{1}2\rangle$ directions. We demonstrate that using As_2 at low substrate temperature also results in triangular GaAs(111)A TSQDs, but with "B-step" edges perpendicular to the three $\langle 11\bar{2}\rangle$ directions. We can therefore invert the crystallographic orientation of these triangular nanostructures, simply by switching between As_4 and As_2. At higher substrate temperatures, GaAs(111)A TSQDs grown under As_2 develop with a hexagonal base. Compared with triangular dots, the higher symmetry of hexagonal TSQDs may reduce fine-structure splitting on this (111) surface, a requirement for robust photon entanglement. Regardless of shape, GaAs(111)A TSQDs grown under As_2 exhibit superior optical quality.

Introduction and Background

Self-assembled quantum dots (QDs) are routinely grown from compressively strained materials on (100)-oriented surfaces by molecular beam epitaxy (MBE). These QDs exhibit highly tunable structural and optoelectronic properties, high crystalline quality, formation via a single processing step, and compatibility with semiconductor device architectures and processing lines.[1–4] Emerging research fronts and device applications have spurred efforts to extend the range of materials systems within which one can synthesize QDs. Example materials systems include (111)-oriented QDs, which have a low fine structure splitting (FSS) for quantum information applications,[5–8] and tensile-strained QDs (TSQDs), which offer band structure engineering capabilities for long wavelength optoelectronics and a potential route towards direct band gap Ge.[9–13]

GaAs/InAlAs(111)A TSQDs were the first optically active nanomaterials to combine the benefits of epitaxial self-assembly, tensile strain, and (111)-orientation.[8] GaAs(111)A TSQDs are dislocation-free, structurally and optically tunable, emit light below the bulk GaAs band edge due to the residual tensile strain, and exhibit low FSS.[14–17] Recent studies describe how GaAs(111)A TSQD properties depend on various MBE growth parameters: deposition amount (in monolayers (MLs)), substrate temperature (T_{SUB}), growth rate, and group V/III flux.[16,17]

This is an author-produced, peer-reviewed version of this article. The final, definitive version of this document can be found online at *Semiconductor Science and Technology*, published by IOP Publishing. Copyright restrictions may apply. https://doi.org/10.1088/1361-6641/aba6e0.

To date however, all GaAs(111)A TSQDs have been grown using tetrameric arsenic (As_4).[8,12,16–18] Most growers today use As_2 rather than As_4 for MBE of III-V semiconductors. However, the original studies that identified the MBE conditions required to grow high quality material on (111) surfaces predated the widespread availability of valved arsenic crackers to generate dimeric As_2.[19–22] As a result, those authors had no choice but to use As_4.[19–22] The use of As_4 for existing work on (111)-oriented TSQDs followed directly from that historical precedent.[8,12,16–18,23]

Researchers have shown that choice of arsenic species can affect photoluminescence (PL) intensity,[24,25] PL linewidth, [26,27] non-radiative interface recombination,[28] the occurrence of deep electron traps,[29] auto-compensation of amphoteric dopants like Si,[29,30] and surface morphology.[31,32] For bulk GaAs(111)A, the As_2 incorporation coefficient (S_{As2}) is larger than that of As_4 (S_{As4}).[30] PL emission from (100)-oriented QDs is also strongly influenced by choice of arsenic species.[26,33–36] On (100), QDs grown with As_4 tend to be more elongated than QDs grown with As_2, with QD size and areal density also impacted.[26,33,34,36]

Clearly, the choice of arsenic species during MBE growth is an important growth variable. We therefore wanted to compare the impact of using As_4 or As_2 on the growth and properties of GaAs/InAlAs(111)A TSQDs, to ascertain whether there exists some benefit to using one molecular species over the other. In this paper we demonstrate that GaAs/InAlAs(111)A TSQD self-assembly still occurs when using As_2. We compare the resulting GaAs TSQDs to equivalent TSQDs grown with As_4. This simple change from As_4 to As_2 results in different nucleation and growth physics, and as a result, more control over TSQD structure, the option to grow either triangular or hexagonal TSQDs, and improved PL emission.

Methods

We use solid-source MBE to grow GaAs(111)A TSQDs within $In_{0.52}Al_{0.48}As$ top and bottom barriers, lattice matched to semi-insulating Fe-doped InP(111)A substrates. First we grow 50nm of lattice-matched $In_{0.53}Ga_{0.47}As$ as a smoothing layer,[23] followed by the 200 nm InAlAs bottom barrier. We have previously reported the optimal growth parameters for InAlAs and InGaAs on InP(111)A.[16,23] GaAs(111)A TSQDs form spontaneously on InAlAs(111)A via a modified Stranski-Krastanov (SK) growth mode. The critical thickness for the 2D-to-3D growth transition is 2.5 ML, but the wetting layer continues to grow even after the TSQDs have begun to self-assemble.[17] For TSQD growth, the GaAs deposition rate is 0.075 ML/sec, with an As:Ga beam equivalent pressure (BEP) ratio of 75, growth conditions favorable for producing high quality TSQDs.[16] We grow GaAs(111)A TSQD samples in the range 485 ºC $\leq T_{SUB} \leq$ 570 ºC. For growth under As_4 and As_2 we used arsenic cracker temperatures of 600 °C and 900 °C, respectively. The GaAs TSQDs are capped with a 50 nm InAlAs top barrier, followed by another layer of GaAs TSQDs for structural analysis with tapping-mode atomic force microscopy (AFM). We use the buried layer of GaAs TSQDs for optical analysis by PL.

We use AFM to explore sample surface morphology, focusing in particular on the shape and size of the TSQDs. By analyzing multiple AFM images of each sample, we compile statistics of average TSQD height, diameter, and areal density as a function of the MBE growth conditions. Note that for these non-

This is an author-produced, peer-reviewed version of this article. The final, definitive version of this document can be found online at *Semiconductor Science and Technology*, published by IOP Publishing. Copyright restrictions may apply. https://doi.org/10.1088/1361-6641/aba6e0.

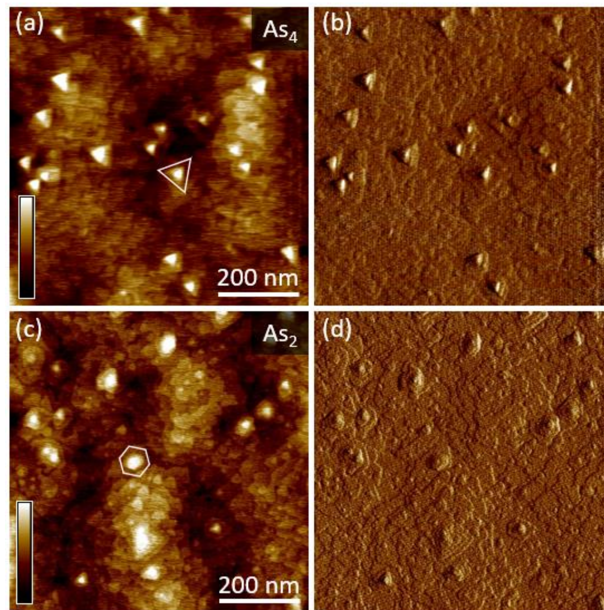

Figure 1: AFM images of GaAs (111)A TSQDs (1 μm², 2 nm height bar). (a, b) show 3 ML GaAs TSQDs deposited under As_4. (c, d) show 4.5 ML GaAs TSQDs deposited under As_2. All other MBE growth conditions are the same. AFM height images (a, c) provide information on QD size, shape, and spacing. AFM amplitude images (b, d) enhance the appearance of QD edges. Using As_4 produces only triangular TSQDs (a, b), while using As_2 produces a mixture of triangular and hexagonal TSQDs (c, d).

circular TSQDs, "diameter" refers to twice the distance from dot center to vertex. We carry out PL measurements at 7 K, using a laser wavelength of 532 nm and an excitation density of 80 W/cm².

Results and Discussion

We grew an initial pair of GaAs(111)A TSQD samples under identical MBE growth conditions (T_{SUB} = 485 °C, growth rate = 0.075 ML/sec, As:Ga BEP ratio = 75), except that we used As_4 for one, and As_2 for the other. Both arsenic species give rise to GaAs TSQD self-assembly. When we compare the resulting GaAs TSQDs with conventional, compressively strained QDs grown on (100) surfaces, they have low average height (< 1.2 nm), large diameter (> 60 nm), and low areal density ($< 5 \times 10^8$ cm^{-2}) (Figs. 1(a) & (c)). These size and density characteristics are consistent with previous research on GaAs(111)A TSQDs.[16]

Figs. 1(b) & (d) show the AFM amplitude (error) images corresponding to Figs. 1(a) & (c). AFM amplitude images, provide higher contrast for changes in surface height, for example at step edges and QD facets, and as a result allow us to better visualize the shapes of these self-assembled GaAs nanostructures.[37] Figs. 1(a)–(b) show that the TSQDs grown under As_4 are always triangular, as seen in previous studies of GaAs(111)A TSQDs.[8,16,17] In contrast, Figs. 1(c)–(d) reveal that TSQDs grown under As_2 consist of a mixture of triangles and hexagons.

This is an author-produced, peer-reviewed version of this article. The final, definitive version of this document can be found online at *Semiconductor Science and Technology*, published by IOP Publishing. Copyright restrictions may apply. https://doi.org/10.1088/1361-6641/aba6e0.

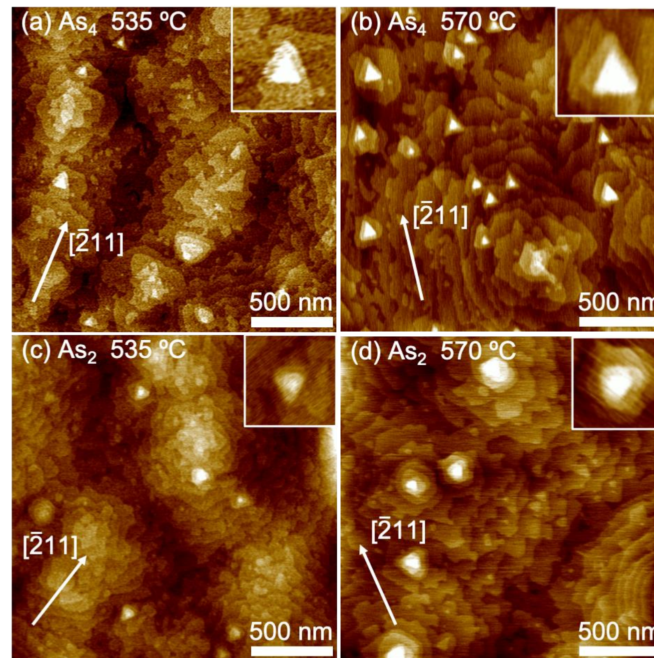

Figure 2: 2×2 μm^2 AFM images showing the appearance of 3.5 ML GaAs (111)A TSQDs as a function of T_{SUB} and arsenic species: (a) GaAs TSQDs grown at 535 °C under As_4;; (b) GaAs TSQDs grown at 570 °C under As_4; (c) GaAs TSQDs grown at 535 °C under As_2; and (d) GaAs TSQDs grown at 570 °C under As_2. All other MBE growth conditions are the same. In (a)–(b), using As_4 produces only triangular TSQDs, while in (c)–(d), using As_2 produces a mixture of triangular and hexagonal TSQDs. Insets are 250×250 nm^2 AFM images of individual QDs from each sample, oriented so that the $[\bar{2}11]$ direction points vertically. All AFM images have a 2 nm height scale.

We were intrigued by the possibility that one could select whether to grow triangular or hexagonal TSQDs, simply by selecting a particular arsenic species (Fig. 1). Some examples of similar shape transitions exist in the literature for the homoepitaxial growth of metals,[38–41] and unstrained GaAs(111)A QDs grown by droplet epitaxy.[42] However, there are no previous demonstrations of shape transitions like this in strain-driven self-assembled QD materials systems, and no existing reports of hexagonal TSQDs.

To investigate this effect further, we therefore grew a series of TSQD samples under As_4 and As_2 at 535 ºC ≤ T_{SUB} ≤ 570 ºC, since TSQD crystal quality improves in this temperature range.[16] We found that TSQDs grown under As_4 at 535 °C are all triangular in shape, just as at 485 °C (Fig. 2(a)). At 570 °C, most TSQDs were still triangular (Fig. 2(b)), but we noted a small population that were hexagonal. For TSQDs grown under As_2 at 535 °C, most were triangular (Fig. 2(c)), but a significant minority were hexagonal in shape. By 570 °C, the vast majority of TSQDs were hexagonal, (Fig. 2(d)) with only occasional triangular TSQDs (Table 1).

When we compared the crystallographic orientations of GaAs TSQDs grown at T_{SUB} = 535 °C, we found that the triangular dots formed under As_4 are inverted compared to those grown with As_2. In Fig. 2(a), the triangular TSQDs grown under As_4 are bounded by "A-steps," perpendicular to the $[\bar{1}2\bar{1}]$, $[2\bar{1}\bar{1}]$, and $[\bar{1}\bar{1}2]$ directions. In Fig. 2(c), the triangular TSQDs grown under As_2 are bounded by "B-steps,"

This is an author-produced, peer-reviewed version of this article. The final, definitive version of this document can be found online at *Semiconductor Science and Technology*, published by IOP Publishing. Copyright restrictions may apply. https://doi.org/10.1088/1361-6641/aba6e0.

Table 1: Summary of TSQD step-edge orientations as a function of arsenic species and substrate growth temperature. We did not categorize TSQDs that were not clearly triangular or hexagonal. Errors indicate the standard deviation in the percent of each type of TSQD observed in various AFM images for each sample.

T_{SUB}	As-species	A-step triangles (%)	Hexagons (%)	B-step triangles (%)
535 °C	As_4	100	0	0
	As_2	0	35±7	65±9
570 °C	As_4	83±5	17±5	0
	As_2	10±9	90±8	0

perpendicular to $[11\bar{2}]$, $[1\bar{2}1]$, and $[\bar{2}11]$. As T_{SUB} is raised to 570 °C, the triangular TSQDs grown under As_4 maintain their A-step orientation (Fig. 2(c)). The hexagonal TSQDs that form at T_{SUB} = 570 °C under As_2 have both A- and B-step edges (Fig. 2(d)).

Fig. 3(a) summarizes the crystallographic directions of the A- and B-steps for GaAs islands on the (111)A surface. Note that in the absence of any surface reconstruction, these GaAs(111)A islands are always bounded by As atoms. On this surface orientation, As atoms have three "upward" pointing bonds with Ga atoms in the same layer, and one out-of-plane bond with a Ga atom in the layer below (Fig. 3(b)). In contrast, the Ga atoms form three bonds "downwards" with As atoms in the same layer, and have one dangling bond pointing up out of the plane (not shown). A Ga atom at the periphery of the island would not form a bond with the surface below and so terminating the island edge with Ga atoms would be unstable. However, because MBE growth takes place under an excess flux of As, it is usually assumed that a Ga atom joining an island edge is stabilized immediately by the addition of an As atom that bonds

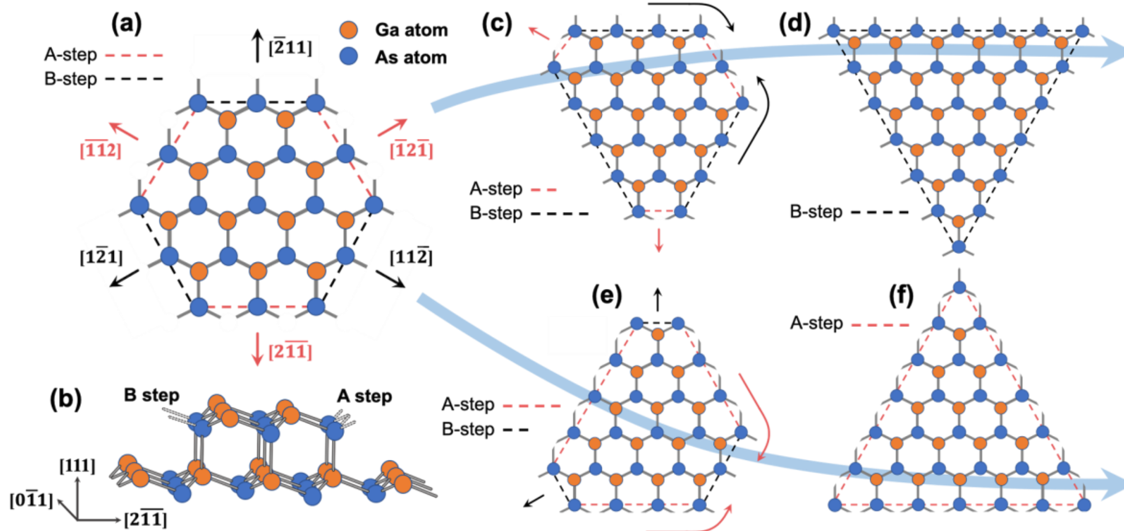

Figure 3: (a) Plan view of an unreconstructed GaAs(111)A island. The crystallographic orientation of the A-steps (red) and B-steps (black) are shown. (b) Cross-sectional view of an unreconstructed GaAs(111)A island in the [0$\bar{1}$1] direction, showing the differences at the A- and B-steps in terms of dangling bonds (shown as dashed lines) and atomic arrangements. (c) If the net edge diffusion of adatoms is from B-steps to A-steps (black arrows), then the A-steps will grow faster (red arrows), getting shorter as they do so, while the B-steps get longer. (d) This process culminates in the formation of a triangular island terminated by B-steps. (e) In contrast, if net adatom diffusion is from A-steps to B-steps (red arrows), the result is the preferential growth at the B-steps (black arrows), and the lengthening of the A-steps. (f) Under this scenario, the outcome is the formation of a triangular island bounded by A-steps.

This is an author-produced, peer-reviewed version of this article. The final, definitive version of this document can be found online at *Semiconductor Science and Technology*, published by IOP Publishing. Copyright restrictions may apply. https://doi.org/10.1088/1361-6641/aba6e0.

with both that Ga atom and with a Ga atom on underlying surface. This As atom then marks the new edge of the island, explaining why these islands always have As atoms at the periphery.

Previous experimental and computational studies show that when growth is kinetically limited, which is usually the case during MBE growth, islands bounded by B-steps often form preferentially.[38–42] Under these conditions, B-step islands are favored for three reasons.[38–40,42,43] First, each As atom at an A-step on the (111)A surface has two bonds to neighboring Ga atoms, one in the same atomic layer and one in the layer below (Fig. 3(b)). At a B-step however, each As atom has three bonds to neighboring Ga atoms, two in the same atomic layer and one in the layer below (Fig. 3(b)). Since the As atoms defining a B-step have more complete bonds than those at an A-step, the cohesive energy of the B-step (defined as the energy required to break the atoms of the solid into isolated atomic species[44]) is higher. B-steps are hence more stable, and so B-step islands are favored.

Second, B-steps have a higher edge diffusion coefficient, efficiently transporting adatoms to neighboring A-steps. As a Ga adatom diffuses along the edge of an island, it moves from one bonding site (local potential well) to another by crossing a potential barrier.[45] The lower this potential barrier, the higher the adatom diffusion coefficient. Each bonding site on a B-step corresponds to an As atom with a single dangling bond, while at an A-step the As atoms at the bonding sites have two dangling bonds (Fig. 3(b)). The result is a weaker interaction between Ga adatoms and the As atoms on B-steps, and so these bonding sites are associated with shallower potential wells than at A-steps. These shallower wells mean a lower potential barrier between bonding sites on a B-step, raising the edge diffusion coefficient compared with at an A-step. The outcome is that Ga adatoms diffuse rapidly along B-steps until they reach a neighboring A-step, where diffusion is slower.

Third, for diffusion to occur between A- and B-steps, adatoms must pass around a corner of the island. Several studies have shown that this corner diffusion process is anisotropic: the probability of an adatom crossing from a B-step to an A-step is higher than from an A-step to a B-step (Fig. 3(c)).[39,41,42,46] Indeed, evidence exists that anisotropic corner diffusion may play the most important role of these three components in dictating final island shape.[39,41]

The net result of these three factors is that during kinetically limited growth, the A-steps grow faster than the B-steps. As a result, the A-steps grow out, get shorter (Fig. 3(c)), and eventually disappear. A triangular island is left behind, bounded by B-steps (Fig. 3(d)),[36,38–40,42,43] just as we observe for GaAs(111)A TSQDs grown under As_2 at T_{SUB} = 535 °C (Fig. 2(c)).

There are however situations where triangular islands bounded by A-steps can form, just as we see for GaAs(111)A TSQDs grown under As_4 (Figs. 2(a)–(b)).[38,41] Ovesson *et al*. showed that simply reversing the corner diffusion anisotropy is sufficient to switch growth from B-step islands to A-step islands.[41] If the net edge diffusion of adatoms inverts from the A-steps to the B-steps, then the B-steps will grow preferentially, lengthening the A-steps (Fig. 3(e)). The eventual outcome is the formation of triangular islands bounded by A-steps (Fig. 3(f)). Michely *et al.* show that one can use T_{SUB} to invert the A-step and

Table 2: (111)A surface arsenic incorporation coefficients for As_4 and As_2 as a function of T_{SUB}, from Tok *et al*.[30] S_{As4} is roughly half that of S_{As2}, regardless of temperature.

	280 °C	470 °C	535 °C	560 °C	570 °C
S_{As4}	0.5	0.24	0.11	0.09	0.08
S_{As2}	1.0	0.50	0.25	0.19	0.18

This is an author-produced, peer-reviewed version of this article. The final, definitive version of this document can be found online at *Semiconductor Science and Technology*, published by IOP Publishing. Copyright restrictions may apply. https://doi.org/10.1088/1361-6641/aba6e0.

B-step growth rate anistotropy.[38] At lower T_{SUB}, adatom diffusion conditions are such that A-step islands grow preferentially. However, we see the A-step islands in Figs. 2(a)–(b) forming at the same or higher substrate temperature to the B-step islands in Fig. 2(c). T_{SUB} cannot therefore be responsible for the observed change from A-step to B-step islands.

The critical difference seems to be the arsenic species, and it is therefore critical to understand how the presence of As_4 or As_2 affects Ga adatom diffusion rates along A- and B-steps. While As_2 molecules dissociate directly on the epitaxial surface, incorporation of arsenic from As_4 is a second order process involving pairs of As_4 molecules at adjacent bonding sites.[47,48] At low T_{SUB} on (111)A surfaces, the As_2 incorporation coefficient, $S_{As2} = 1$, while for As_4, $S_{As4} = 0.5$. However, unlike the (100) surface, arsenic incorporation on (111) surfaces is temperature dependent. Both S_{As2} and S_{As4} fall as T_{SUB} is increased: at 560 °C, $S_{As2} \sim 0.2$, and $S_{As4} \sim 0.1$ (Table 2).[30] This decrease in S_{As4} and S_{As2} explains why at typical growth temperatures, a high As:Ga flux ratio is necessary for high epitaxial quality on (111) surfaces.[23,30]

In a study of InAsP growth, Zhang *et al.* noted that when As incorporation is lower, for example when using As_4 instead of As_2, diffusion of the Group III adatoms is enhanced at A-steps. This leads to preferential bonding at B-steps and hence they grow faster than the A-steps.[49] We propose that this same mechanism is responsible for the appearance of A-step islands when we grow with As_4.

Hexagonal islands occur when T_{SUB} becomes high enough that the thermal energy eclipses the differences in binding energies and diffusion rates at the A- and B-steps. At such high temperatures, the atoms gain sufficient energy to detach from the A- and B-steps of existing islands, generating kinks. These kinks lower the chemical potential of the steps, and break down the competing edge diffusion processes.[40] The result is an island in equilibrium, bounded by both A- and B-steps, whose hexagonal shape reflects the underlying three-fold symmetry of the (111)A surface.[38–40,50] We believe this is the mechanism responsible for higher percentage of hexagonal TSQDs that form under As_2, as T_{SUB} is increased from 535 °C to 570 °C. This mechanism also explains the appearance of occasional hexagonal TSQDs at T_{SUB} = 570 °C for growth under As_4 (Table 1).

Increasing T_{SUB} from 535 ºC to 570 ºC does not significantly change average TSQD height for samples grown with either As_4 or As_2 (Fig. 4(a)). For $T_{SUB} \leq 560$ °C, the average diameter of TSQDs grown with As_4, and As_2 are essentially identical, with both increasing as we raise T_{SUB} in this range (Fig. 4(b)). At T_{SUB} = 570 °C however, we see a marked divergence in the response of TSQDs grown under As_4 and As_2. The average diameter of TSQDs grown with As_2 continues to increase monotonically as we raise T_{SUB} (Fig. 4(b)). Raising T_{SUB} increases the mean adatom diffusion length, promoting adatom attachment to existing islands rather than the nucleation of new QDs.[1,14,51,52] The result of raising T_{SUB} under As_2 is therefore to produce GaAs TSQDs with larger average size and lower areal density.[53] In contrast, TSQDs grown with As_4 at T_{SUB} = 570 °C undergo a marked reduction in their average diameter (Fig. 4(b)).

A possible explanation for this difference in TSQD self-assembly with As_4 and As_2 is again found in the disparity between the values of S_{As4} and S_{As2} (Table 2). $S_{As2} \approx 2S_{As4}$ at all values of T_{SUB}, meaning that for the same flux, the surface arsenic concentration will be higher when using As_2 than As_4. Growth under As_2 is therefore expected to result in (111)A surfaces with the arsenic-rich, As-trimer reconstruction.[54,55] In contrast, at high T_{SUB} the lower incorporation of As_4 could push growth into a Ga-rich regime where the Ga-vacancy surface reconstruction is most stable.[54] Previous reports have shown bulk GaAs(111)A grown under As_4 transiting to a Ga-rich surface when heated above 550 °C.[56] Calculations suggest that the energy barrier to Ga adatom diffusion is four times larger on the Ga-vacancy reconstruction than the As-

This is an author-produced, peer-reviewed version of this article. The final, definitive version of this document can be found online at *Semiconductor Science and Technology*, published by IOP Publishing. Copyright restrictions may apply. https://doi.org/10.1088/1361-6641/aba6e0.

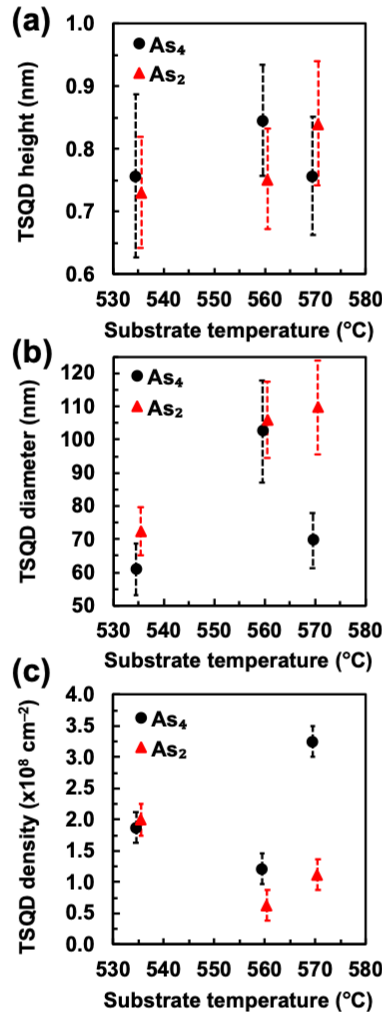

Figure 4: Average (a) height, (b) diameter and (c) areal density of GaAs/InAlAs(111)A TSQDs grown with As_4 (black) and As_2 (red), as a function of T_{SUB} (error bars represent one standard deviation). For clarity, data points at the same T_{SUB} are offset horizontally by 1 °C.

trimer reconstruction.[45] Lower adatom diffusion results in QDs with smaller diameter and higher areal density.[1,14,16,52] A sudden transition at T_{SUB} = 570 °C from the As-trimer to Ga-vacancy reconstruction for growth under As_4 could therefore explain the abrupt reduction in TSQD diameter that we see in Fig. 4(b).

If this is the correct mechanism, the appearance of the Ga-vacancy reconstruction at T_{SUB} = 570 °C should also increase TSQD areal density for samples grown under As_4. This is indeed what we see (Fig. 4(c)). Regardless of As species, for $T_{SUB} \leq 560$ °C, we see a monotonic decrease in TSQD density as the temperature is raised, as expected for increased Ga adatom diffusion.[14,16] However, at T_{SUB} = 570 °C, TSQDs grown under As_4 undergo a threefold increase in density, consistent with a sudden drop in adatom diffusion. For comparison, the density of TSQDs grown under As_2 does not change (to within error) between T_{SUB} = 560 °C and 570 °C (Fig. 4(c)).

PL spectroscopy of the various samples consistently show enhanced emission intensity for TSQDs grown using As_2 compared with As_4 (Fig. 5). To aid comparison, in each case we have normalized the PL spectra to the intensity of the InAlAs barrier peak at 856 nm since this should be identical across samples.

This is an author-produced, peer-reviewed version of this article. The final, definitive version of this document can be found online at *Semiconductor Science and Technology*, published by IOP Publishing. Copyright restrictions may apply. https://doi.org/10.1088/1361-6641/aba6e0.

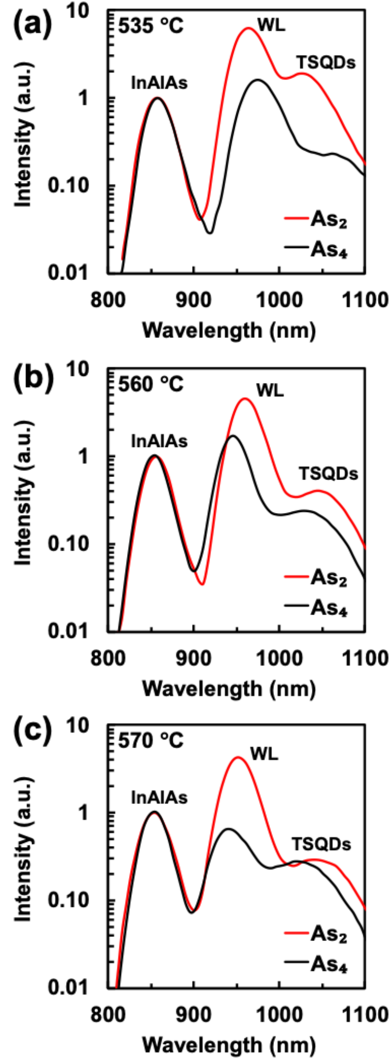

Figure 5: 7 K PL emission spectra from GaAs(111)A TSQDs samples growth with As_2 (red) and As_4 (black) at T_{SUB} = (a) 535 °C, (b) 560 °C, and (c) 570 °C. Spectral intensities are normalized to the bulk InAlAs peak.

The peak at 941–975 nm corresponds to the tensile-strained GaAs wetting layer (WL), while the smaller peak at 1009–1040 nm comes from the GaAs TSQDs. Ref. [17] details how these peaks were assigned.

These spectra contrast with conventional InAs/GaAs(100) QDs whose areal densities are typically in the 10^{10} cm^{-2} range.[57] Once the InAs dots begin to form, PL from the QDs dominates, while emission from the WL is difficult to resolve.[57] The opposite is true for the GaAs TSQD spectra in Fig. 5. For all samples, emission from the tensile-strained GaAs WL is more intense than from the GaAs TSQDs (Fig. 5). The reason is that the GaAs TSQD areal densities are in the 10^8 cm^{-2} range (see Fig. 4(c)), i.e., 100× lower than for InAs/GaAs(100) QDs. PL emission from fewer TSQDs per unit area means that the TSQD peaks are weaker, and so the WL peaks dominate these spectra (Fig. 5).

However, our primary interest is to compare the effect of As_4 and As_2 on the optical properties of these samples. Plotting the intensity of the WL peaks in Fig. 5, shows that, regardless of T_{SUB}, the use of As_2 during growth results in brighter PL emission compared with the use of As_4 (Fig. 6(a)). We can perform a similar comparison for the PL intensity of the GaAs TSQD peaks, but we must first account for the

This is an author-produced, peer-reviewed version of this article. The final, definitive version of this document can be found online at *Semiconductor Science and Technology*, published by IOP Publishing. Copyright restrictions may apply. https://doi.org/10.1088/1361-6641/aba6e0.

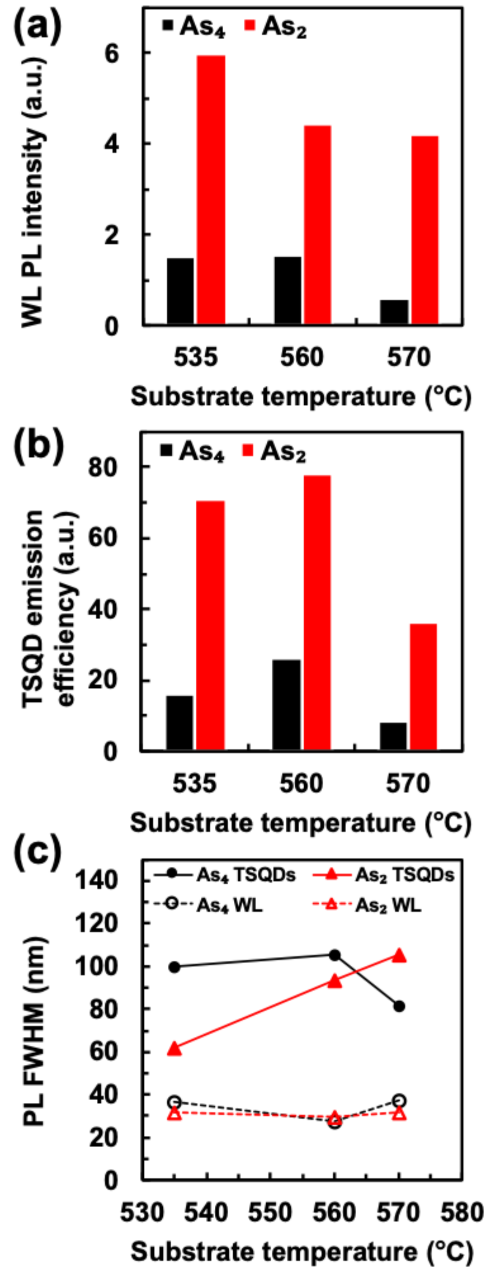

Figure 6: The impact of arsenic species on (a) tensile-strained GaAs WL PL intensity, and (b) GaAs(111)A TSQD PL emission efficiency as a function of T_{SUB}. (c) FWHM of the GaAs(111)A TSQD and WL PL peaks as a function of T_{SUB} and arsenic species.

variation in TSQD areal density from sample to sample. For a given laser spot size, the more TSQDs that are excited, the more photons will be emitted. This is particularly important for samples grown under As_4, given the increase in TSQD density we see at T_{SUB} = 570 °C (Fig. 4(c)). We therefore use a metric we refer to as *emission efficiency*, which is given by the integrated area of the TSQD PL peak, divided by the areal density of TSQDs on that sample.[16]

Plotting emission efficiency shows that regardless of T_{SUB}, PL emission from GaAs TSQDs grown with As_2 is more intense than from TSQDs grown with As_4 (Fig. 6(b)). Despite the higher areal density of the As_4-grown TSQDs at T_{SUB} = 570 °C, the As_2-grown TSQDs still have higher emission efficiency. TSQD

This is an author-produced, peer-reviewed version of this article. The final, definitive version of this document can be found online at *Semiconductor Science and Technology*, published by IOP Publishing. Copyright restrictions may apply. https://doi.org/10.1088/1361-6641/aba6e0.

emission efficiency falls off for both As_2 and As_4 samples as we raise T_{SUB} from 560 °C to 570 °C. This behavior shows that material quality is compromised, most likely as a result of the very low As incorporation coefficients of both arsenic species at this high temperature (Table 2).[30,32]

We can therefore conclude that the use of As_2 during the growth of these TSQD samples significantly improves the optical quality of the GaAs in both the tensile-strained WL and in the TSQDs themselves. Specifically, the use of As_2 increases WL emission intensity by 3–7× and TSQD emission efficiency by 3–4×, compared with the use of As_4 (Figs. 6(a)–(b)). In general, higher PL intensity is an indicator of lower non-radiative recombination and improved material quality. Researchers have long associated the pairwise incorporation mechanism for As_4 with increased levels of point defects,[48] and shown that defect densities can be reduced by using As_2 instead.[58]

The spectral linewidth of the WL PL peaks, defined as the full width at half maximum (FWHM), remains constant regardless of T_{SUB} and the arsenic species used (Fig. 6(c)). This tells us that the width uniformity of the WL quantum well is robust against these changes in the MBE growth parameters. For samples grown at $T_{SUB} \leq 560$ °C, the FWHM of the TSQD PL peaks, is narrower for samples grown with As_2 than with As_4 (Fig. 6(c)). In general, for an array of QDs, a narrower FWHM is consistent with a more uniform dot size distribution, and is a positive attribute for many light emission applications. The overall trend for both As_4- and As_2-grown TSQDs is for larger FWHM as T_{SUB} is raised, consistent with an increase in Ostwald ripening as adatom diffusion is enhanced. However, at $T_{SUB} = 570$ ºC the trend for TSQDs grown under As_4 is reversed, and a lower FWHM suggests that they are more uniform in size. The transition to the Ga-vacancy reconstruction and the accompanying reduction in Ga adatom diffusion hampers Ostwald ripening. At this high temperature, the result is a slight improvement in size uniformity for TSQDs grown under As_4 compared with As_2.

Conclusions

We can manipulate the shape, size, areal density, and optical emission quality of GaAs/InAlAs(111)A TSQDs during MBE growth through our choice of arsenic species and T_{SUB}. GaAs(111)A TSQDs have three distinct morphologies: A- and B-step triangular TSQDs, and high symmetry hexagonal TSQDs. Which shape arises depends on the relative growth rates of the A- and B-steps. We demonstrate that we can influence these growth rates by growing under As_4 or As_2. At sufficiently high T_{SUB}, differences between the A- and B-step growth rates become negligible, and hexagonal TSQDs appear. We know that higher *structural* symmetry helps to reduce FSS in semiconductor QDs, for example in triangular (111) TSQDs compared to elliptical (100) QDs.[5,6,59,60] In future, we are therefore interested to see if the higher structural symmetry of the hexagonal GaAs(111)A TSQDs we can now grow using As_2, will offer even lower FSS than the triangular GaAs(111)A TSQDs we have investigated to date.[8]

When using As_4, we see evidence for a transition from the As-trimer to the Ga-vacancy surface reconstruction at $T_{SUB} = 570$ °C. This transition seems to be triggered by the particularly low arsenic incorporation coefficient for As_4 compared with As_2 at this high temperature. In all sample sets, growth under As_2 produces samples with better optical quality than As_4. We therefore recommend that for optoelectronic applications, MBE growth of GaAs(111)A TSQDs should be carried out under As_2 instead of As_4. The high symmetries available in these self-assembled nanostructures may prove to be beneficial for quantum optics applications.

This is an author-produced, peer-reviewed version of this article. The final, definitive version of this document can be found online at *Semiconductor Science and Technology*, published by IOP Publishing. Copyright restrictions may apply. https://doi.org/10.1088/1361-6641/aba6e0.

Acknowledgements

This material is based upon work supported by the National Science Foundation under NSF CAREER Grant No. 1555270.

References

[1] B.A. Joyce and D.D. Vvedensky, Mater. Sci. Eng. R **46**, 127 (2004).

[2] S. Franchi, G. Trevisi, L. Seravalli, and P. Frigeri, Prog. Cryst. Growth Charact. Mater. **47**, 166 (2003).

[3] F. Ratto and F. Rosei, Mater. Sci. Eng. R **70**, 243 (2010).

[4] A.P. Alivisatos, Science **271**, 933 (1996).

[5] A. Schliwa, M. Winkelnkemper, A. Lochmann, E. Stock, and D. Bimberg, Phys. Rev. B **80**, 161307(R) (2009).

[6] S. Schulz, M.A. Caro, E.P. O'Reilly, and O. Marquardt, Phys. Rev. B **84**, 125312 (2011).

[7] G. Juska, E. Murray, V. Dimastrodonato, T.H. Chung, S.T. Moroni, A. Gocalinska, and E. Pelucchi, J. Appl. Phys. **117**, 134302 (2015).

[8] C.D. Yerino, P.J. Simmonds, B. Liang, D. Jung, C. Schneider, S. Unsleber, M. Vo, D.L. Huffaker, S. Höfling, M. Kamp, and M.L. Lee, Appl. Phys. Lett. **105**, 251901 (2014).

[9] G. Signorello, S. Karg, M.T. Björk, B. Gotsmann, and H. Riel, Nano Lett. (2012).

[10] M. El Kurdi, G. Fishman, S. Sauvage, and P. Boucaud, J. Appl. Phys. **107**, 013710 (2010).

[11] X. Li, K. Maute, M.L. Dunn, and R. Yang, Phys. Rev. B **81**, 245318 (2010).

[12] P.J. Simmonds and M.L. Lee, J. Appl. Phys. **112**, 054313 (2012).

[13] K.E. Sautter, C.F. Schuck, T.A. Garrett, A.E. Weltner, K.D. Vallejo, D. Ren, B. Liang, K.A. Grossklaus, T.E. Vandervelde, and P.J. Simmonds, J. Cryst. Growth **533**, 125468 (2020).

[14] P.J. Simmonds and M.L. Lee, Appl. Phys. Lett. **99**, 123111 (2011).

[15] P.J. Simmonds, R.B. Laghumavarapu, M. Sun, A. Lin, C.J. Reyner, B. Liang, and D.L. Huffaker, Appl. Phys. Lett. **100**, 243108 (2012).

[16] C.F. Schuck, R.A. McCown, A. Hush, A. Mello, S. Roy, J.W. Spinuzzi, B. Liang, D.L. Huffaker, and P.J. Simmonds, J. Vac. Sci. Technol. B **36**, 031803 (2018).

[17] C.F. Schuck, S.K. Roy, T. Garrett, Q. Yuan, Y. Wang, C.I. Cabrera, K.A. Grossklaus, T.E. Vandervelde, B. Liang, and P.J. Simmonds, Sci. Rep. **9**, 18179 (2019).

[18] P.J. Simmonds, J. Simon, J.M. Woodall, and M.L. Lee, J. Vac. Sci. Technol. B **29**, 03C103 (2011).

[19] Y. Okano, M. Shigeta, H. Seto, H. Katahama, S. Nishine, and I. Fujimoto, Jpn. J. Appl. Phys. **29**, L1357 (1990).

[20] K. Sato, M.R. Fahy, and B.A. Joyce, Jpn. J. Appl. Phys. **33**, L905 (1994).

[21] T. Yamamoto, M. Inai, T. Takebe, and T. Watanabe, J. Vac. Sci. Technol. A **11**, 631 (1993).

[22] D.A. Woolf, D.I. Westwood, and R.H. Williams, Semicond. Sci. Technol. **8**, 1075 (1993).

[23] C.D. Yerino, B. Liang, D.L. Huffaker, P.J. Simmonds, and M.L. Lee, J. Vac. Sci. Technol. B **35**, 010801 (2017).

[24] W.T. Tsang, J.A. Ditzenberger, and N.A. Olsson, IEEE Electron Device Lett. **4**, 275 (1983).

[25] Z.-B. Hao, Z.-Y. Ren, W.-P. Guo, and Y. Luo, J. Cryst. Growth **224**, 224 (2001).

[26] B. Liang, Q. Yuan, L. Su, Y. Wang, Y. Guo, S. Wang, G. Fu, E. Marega Jr., Y.I. Mazur, M.E. Ware, and G. Salamo, Opt. Express **26**, 23107 (2018).

[27] C. Gilfert, E.-M. Pavelescu, and J.P. Reithmaier, Appl. Phys. Lett. **96**, 191903 (2010).

[28] G. Duggan, P. Dawson, C.T. Foxon, and G.W. 't Hooft, J. Phys. **43**, **C5**, 129 (1982).

[29] H. Jung, H. Künzel, and K. Ploog, J. Phys. **43**, **C5**, 135 (1982).

[30] E.S. Tok, T.S. Jones, J.H. Neave, J. Zhang, and B.A. Joyce, Appl. Phys. Lett. **71**, 3278 (1997).

[31] T. Hayakawa, M. Nagai, M. Morishima, H. Horie, and K. Matsumoto, Appl. Phys. Lett. **59**, 2287 (1991).

[32] D.M. Holmes, J.G. Belk, J.L. Sudijono, J.H. Neave, T.S. Jones, and B.A. Joyce, Appl. Phys. Lett. **67**, 2848

This is an author-produced, peer-reviewed version of this article. The final, definitive version of this document can be found online at *Semiconductor Science and Technology*, published by IOP Publishing. Copyright restrictions may apply. https://doi.org/10.1088/1361-6641/aba6e0.

(1995).

[33] T. Sugaya, T. Amano, and K. Komori, J. Appl. Phys. **100**, 063107 (2006).

[34] S. Suraprapapich, S. Panyakeow, and C.W. Tu, Appl. Phys. Lett. **90**, 183112 (2007).

[35] T. Sugaya, S. Furue, T. Amano, and K. Komori, J. Cryst. Growth **301**–**302**, 801 (2007).

[36] A.R. Avery, H.T. Dobbs, D.M. Holmes, B.A. Joyce, and D.D. Vvedensky, Phys. Rev. Lett. **79**, 3938 (1997).

[37] P. Eaton and P. West, *Atomic Force Microscopy*, 1st ed. (Oxford University Press, Oxford, UK, 2010).

[38] T. Michely, M. Hohage, M. Bott, and G. Comsa, Phys. Rev. Lett. **70**, 3943 (1993).

[39] E. Cox, M. Li, P.-W. Chung, C. Ghosh, T.S. Rahman, C.J. Jenks, J.W. Evans, and P.A. Thiel, Phys. Rev. B **71**, 115414 (2005).

[40] B. Lü, G.A. Almyras, V. Gervilla, J.E. Greene, and K. Sarakinos, Phys. Rev. Mater. **2**, 063401 (2018).

[41] S. Ovesson, A. Bogicevic, and B.I. Lundqvist, Phys. Rev. Lett. **83**, 2608 (1999).

[42] M. Jo, T. Mano, M. Abbarchi, T. Kuroda, Y. Sakuma, and K. Sakoda, Cryst. Growth Des. **12**, 1411 (2012).

[43] M.H. Xie, S.M. Seutter, W.K. Zhu, L.X. Zheng, H. Wu, and S.Y. Tong, Phys. Rev. Lett. **82**, 2749 (1999).

[44] X. Li, Nanotechnology **25**, 185702 (2014).

[45] J.N. Shapiro, A. Lin, D.L. Huffaker, and C. Ratsch, Phys. Rev. B **84**, 085322 (2011).

[46] S.C. Wang and G. Ehrlich, Surf. Sci. **239**, 301 (1990).

[47] C.T. Foxon and B.A. Joyce, Surf. Sci. **50**, 434 (1975).

[48] C.T. Foxon, J. Vac. Sci. Technol. B **1**, 293 (1983).

[49] W. Zhang, C. Yi, and A. Brown, J. Vac. Sci. Technol. B **25**, 960 (2007).

[50] M. Schmid, E. Lundgren, G. Leonardelli, A. Hammerschmid, B. Stanka, and P. Varga, Appl. Phys. A **72**, 405 (2001).

[51] V. Shchukin, E. Schöll, and P. Kratzer, in *Semicond. Nanostructures*, edited by D. Bimberg (Springer Berlin Heidelberg, Berlin, Heidelberg, 2008), pp. 1–39.

[52] M. Meixner, R. Kunert, and E. Schöll, Phys. Rev. B **67**, 195301 (2003).

[53] C. Lobo and R. Leon, J. Appl. Phys. **83**, 4168 (1998).

[54] E. Kaxiras, Y. Bar-Yam, J.D. Joannopoulos, and K.C. Pandey, Phys. Rev. B **35**, 9625 (1987).

[55] N. Moll, A. Kley, E. Pehlke, and M. Scheffler, Phys. Rev. B **54**, 8844 (1996).

[56] M.R. Fahy, K. Sato, and B.A. Joyce, Appl. Phys. Lett. **64**, 190 (1994).

[57] R. Leon and S. Fafard, Phys. Rev. B **58**, R1726 (1998).

[58] H. Künzel and K. Ploog, Appl. Phys. Lett. **37**, 416 (1980).

[59] R. Seguin, A. Schliwa, S. Rodt, K. Pötschke, U.W. Pohl, and D. Bimberg, Phys. Rev. Lett. **95**, 257402 (2005).

[60] R. Singh and G. Bester, Phys. Rev. Lett. **103**, 063601 (2009).